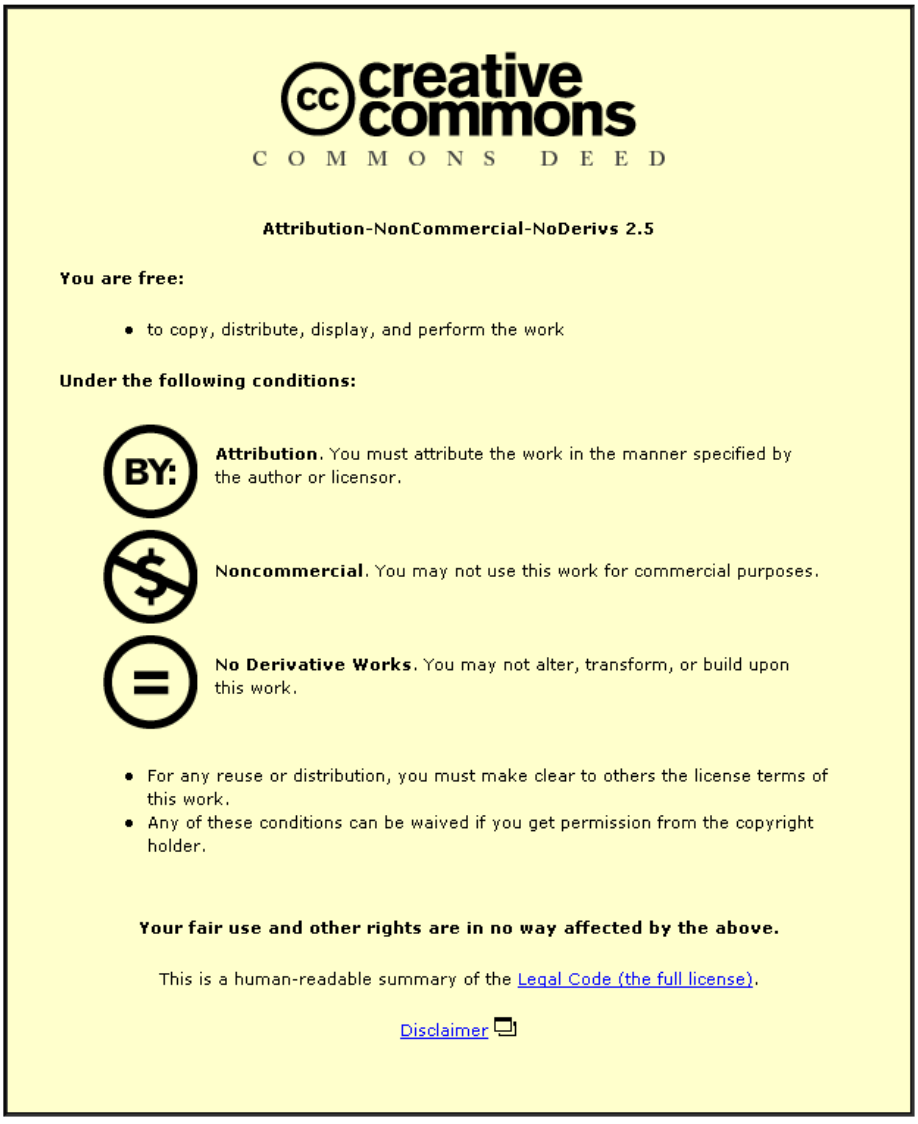

creative commons

COMMONS DEED

Attribution-NonCommercial-NoDerivs 2.5

You are free:

- to copy, distribute, display, and perform the work

Under the following conditions:

Attribution. You must attribute the work in the manner specified by the author or licensor.

Noncommercial. You may not use this work for commercial purposes.

No Derivative Works. You may not alter, transform, or build upon this work.

- For any reuse or distribution, you must make clear to others the license terms of this work.
- Any of these conditions can be waived if you get permission from the copyright holder.

Your fair use and other rights are in no way affected by the above.

This is a human-readable summary of the Legal Code (the full license).

Disclaimer

Friction compensation of an actively restrained clutch for path tracking

L M Lacraru* and **K Bouazza-Marouf**
Wolfson School of Mechanical and Manufacturing Engineering, Loughborough University, Loughborough, UK

The manuscript was received on 22 July 2005 and was accepted after revision for publication on 5 April 2006.

DOI: 10.1243/09596518JSCE186

Abstract: Friction compensation of an electromechanical friction clutch mechanism capable of restraining motion so that various predefined paths can be followed is investigated in this paper. The clutch mechanism is driven by an external source of energy, and a computer-controlled system is used to produce frictional resistance so that a desired motion can be achieved. Unknown stick–slip within the clutch is a critical characteristic of the system, which has to be overcome. Three different controllers are investigated in order to avoid stick–slip at low motion rates. A proportional–derivative controller, a sliding-mode controller, and a computed-torque controller, have been implemented and their performances compared using simulation and experimental analyses. The results demonstrate the effectiveness of the sliding-mode controller and the potential of a computed-torque controller for the motion control in a system with dry friction at low velocities.

Keywords: dry friction, stick–slip, friction compensations, sliding-mode control, electromechanical clutch, path tracking

1 INTRODUCTION

Friction is a commonly studied effect, as it always appears when there is contact between two bodies. However, owing to its non-linearity there are still difficulties in both modelling it and developing control strategies to overcome it [**1**]. At low velocities a periodic process of sticking and sliding can be observed. This phenomenon is known as the stick–slip effect. Stick–slip friction is present to some degree in almost all mechanisms and is often responsible for performance limitations. The effect often results in undesirable dynamic behaviour. Precise position control tasks, such as those found in robotic applications [**2–4**], or in machine tools [**5–7**], are examples of systems affected by this phenomenon. Stick–slip friction puts a lower bound on the performance that can be extracted from a mechanism, such as the minimum velocity achievable and persistent steady state errors. Symptoms of this phenomenon in mechanisms can be anything from jerky motion or limit cycles, to catastrophic instability. All the above examples use the control of direct drive motors in order to perform a task (e.g. positioning or path following). Thus, the objective is to reduce the effect of friction so that the efficiency of the overall mechanism is maximized.

The proposed electromechanical friction clutch is driven by an external source of energy such as gravity or human operator, and a computer-controlled clutch is used to produce resistance so that a desired path can be followed. In this case, the human operator provides the motive force or torque and the motion is controlled indirectly via a clutch mechanism. This type of mechanism can be used in safety critical applications such as robotic- or mechatronic-assisted surgical procedures.

The friction in this case must be used in order to achieve a task such as reaching a predefined position and/or following a predefined path. Thus, the stick–slip phenomenon is even more critical in brake and clutch systems used for precise position or trajectory control.

A good example of a system based on brakes and clutches used for trajectory control is the passive

* *Corresponding author: Wolfson School of Mechanical and Manufacturing Engineering, Loughborough University, Ashby Road, Loughborough LE11 3TU. email: Lucian.Lacraru@gmail.com*

trajectory-enhancing robot (PTER) developed by a group at the Georgia Institute of Technology, USA [**8**, **9**]. The PTER is a passive robot used for path tracking while under human input force. It was found that owing to the stick–slip inherent in the clutches of the PTER, an undesirable discontinuous motion of the manipulator occurred, which cannot be cancelled or diminished. Although several control strategies based on joint torque control have been employed [**10–13**], the manipulator is not able to track smoothly a trajectory any closer than about 4 mm.

For direct drive control systems, several control approaches have been proven to be effective in reducing the effect of friction at low velocities. The broad classes of friction compensation strategies are problem avoidance, non-model-based compensation, and model-based compensation. This paper investigates non-model-based and model-based compensation techniques applied on a clutch mechanism used for path tracking.

Among the non-model-based friction compensation methods, which have been investigated for direct drive control, the following have proven to be quite effective in reducing the effect of undesired friction-related effects at low velocities: high-gain proportional–derivative (PD) control [**14**, **15**], joint torque control [**16–19**], sliding-mode control (SMC) [**20–22**], dither [**23–25**], and impulsive control [**14**, **26**, **27**].

In this paper the PD and SMC methods are investigated as non-model-based friction compensation techniques, and computed-torque control (CTC) as a model-based friction compensation technique. These three methods are developed in section 3 and investigated in section 4 for a mechanism where friction is used in order to follow successfully a predefined path when the motive force cannot be controlled.

2 DESCRIPTION OF THE MECHANISM

An experimental setup of the clutch mechanism, which has been used to investigate the control strategies, is shown in Fig. 1. A pulley-weight system is used to produce a driving torque T_u applied to the main shaft. A braking mechanism is used to restrain the motion of the shaft so that different tasks can be performed (e.g. reach a position or follow a trajectory). This braking mechanism consists of a d.c. motor (6), a connection shaft (7), a lever (8), a cantilever (5), and the brake disc (2). The d.c. motor (6) is used to produce a controllable torque T_{DC}, which is converted into a mechanical force F_N on to the braking disc (2) by the lever (8). The cantilever (5) acts as a frictional pad on to the braking disc (2), thus creating the sliding friction (i.e. frictional force F_f or frictional torque T_f). The braking mechanism that provides the frictional torque T_f is better

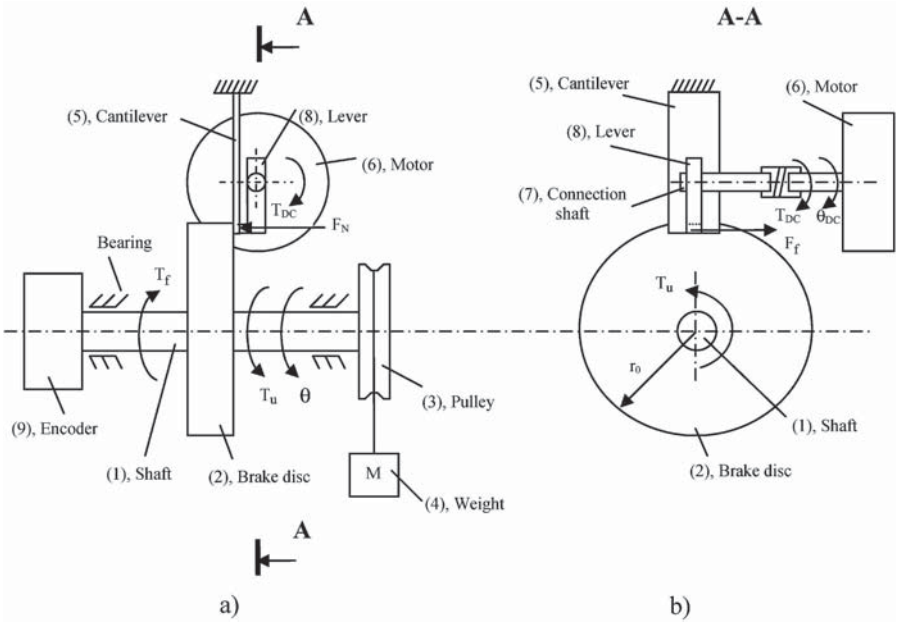

Fig. 1 Schematic diagram of the experimental set-up: (a) front view; (b) side view. The numbers in parentheses refer to the respective item numbers

illustrated in Fig. 1(b). The incremental encoder (9) mounted on the shaft (1) is used to measure the actual angular position θ of the shaft. The control system regulates the angular position θ, to remain as close as possible with respect to a desired motion profile. The clutch parameters are given in Table 1.

A block diagram of the control system is illustrated in Fig. 2, and the equation of motion of the system is given by

$$\ddot{\theta} = J^{-1}\left[MgR_{\mathrm{p}} - \mu(\dot{\theta})\frac{r_{\mathrm{i}}K_{\mathrm{t}}A}{A_{\mathrm{lever}}R_{\mathrm{a}}r_{\mathrm{c}}}v_{\mathrm{a}}(t) - C_{\mathrm{d}}\dot{\theta}\right] \qquad (1)$$

where J denotes the inertia of the clutch, M is the mass of the load on the pulley, g represents the gravitational acceleration, $v_{\mathrm{a}}(t)$ represents the applied voltage, C_{d} is the viscous coefficient in the dynamic system, r_{i} is the inner radius of the brake disc, K_{t} represents the motor torque constant, A denotes the area of the contact between the brake pad and brake disc, A_{lever} is the area of the tip of the lever, R_{a} is the motor's armature resistance, r_{c} is the distance between the centre of the motor shaft and the contact on the brake disc, and $\mu(\dot{\theta})$ denotes the coefficient of friction. The coefficient of friction $\mu(\dot{\theta})$ is modelled as

$$\mu(\dot{\theta}) = [\mu_{\mathrm{d}} + (\mu_{\mathrm{s}} - \mu_{\mathrm{d}})\,\mathrm{e}^{-|\dot{\theta}/\dot{\theta}_{\mathrm{S}}|^{\delta}})\,\mathrm{sgn}(\dot{\theta}) \qquad (2)$$

where μ_{d} represents the dynamic coefficient of friction, μ_{s} denotes the static coefficient of friction, $\dot{\theta}_{\mathrm{S}}$ is the Stribeck velocity, and δ is the Stribeck coefficient. The parameters $\dot{\theta}_{\mathrm{S}}$ and δ are specified so that stick–slip is promoted. The values of these parameters are listed in Table 1 together with all other parameters of the experimental clutch system.

3 FRICTION COMPENSATION

The aim is to control the electromechanical friction clutch in order to follow smoothly and accurately a velocity command of 2°/s. The main challenge is the overcoming of the stick–slip effect, which puts

Table 1 Clutch parameters

Notation	Value	Description
J	0.0017 kg m²	Total moment of inertia of clutch + a mass M of 0.2 kg
R_{p}	0.024 m	Radius of pulley
r_{o}	0.05 m	Radius of the brake disc
r_{i}	0.045 m	Inner radius of the brake disc
r_{c}	0.034 m	Distance between centre of the motor shaft and the contact point on the disc
L	0.03 m	Width of the friction pad
h	0.0055 m	Height of the rectangular part of the brake pad
A_{lever}	0.032 m²	Area of a rectangular shape of the mechanical lever
A	0.040 m²	Area of the contact between the brake pad and the brake disc
K_{COF}	0.14	Constant of the coefficient of friction
C_{d}	0.001	Viscous damping coefficient in the clutch system
γ	0.6 rad	Angle of the segment of the proposed annular brake pad
μ_{s}	0.2	Static coefficient of friction
μ_{d}	0.15	Dynamic coefficient of friction
$\dot{\theta}_{\mathrm{S}}$	0.001	Stribeck velocity
δ	1	Stribeck coefficient

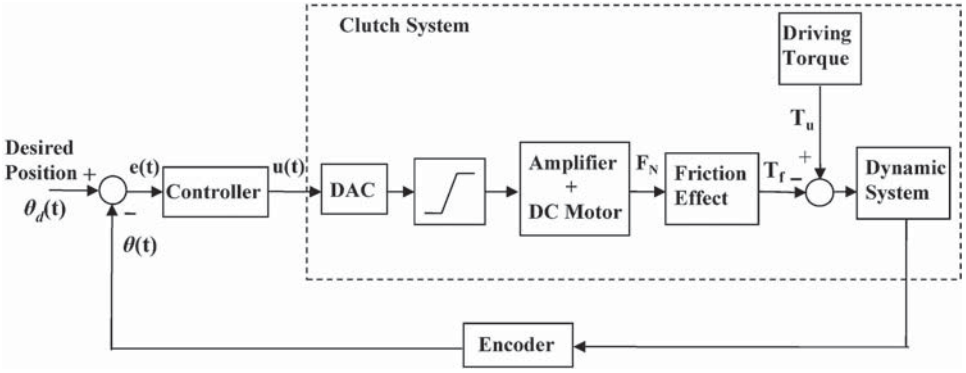

Fig. 2 System block diagram

a lower bound on the performance that can be extracted from the mechanism, such as the minimum velocity achievable and persistent steady state errors. While stick–slip is of great importance in mechanisms with direct actuation such as those found in robotic applications [**2–4**], or in machine tools [**5–7**], it is even more important in brake and clutch systems used for precise position or trajectory control.

In this section, three friction compensation techniques are developed in an attempt to diminish the stick–slip friction effect within a clutch mechanism used for path tracking. These three methods are PD control, CTC, and SMC.

High-gain PD control is among the most common techniques employed for friction compensation. It has been experimentally observed that sufficiently stiff and/or damped systems do not exhibit stick–slip [**14**]. In a control context, this is accomplished by increasing the PD gains. The PD gains can be chosen to provide a reasonably sized domain of attraction so that the equilibrium point of steady sliding remains attractive and asymptotically stable under expected perturbations, as demonstrated by Dupont [**15**].

The CTC method makes direct use of the complete dynamic model of a system to cancel not only the effects of gravity, but also the Coriolis force, the centrifugal force, friction, and the manipulator inertia tensor [**28**]. Thus, accurate estimation of the system parameters is required, which is very challenging in a machine with friction. Even though the method is widely used for robotic systems with satisfactory results, it has not been demonstrated to be effective for a braking–clutching mechanism used for position or trajectory control.

A controller based on sliding-mode theory has some features that make it a good candidate as an active friction compensation technique. Sliding-mode controllers are well known to be robust against bounded unstructured modelling errors. However, they are also known for the fact that they tend to cause chattering. The chattering generated by sliding-mode controllers is not always advantageous but can be effective in removing stiction. SMC was implemented by several workers [**20–22**] with good results for compensating friction-related effects. Lee *et al.* [**20**] showed in simulations that, for Coulomb friction with stick-slip in an ultra-precision machining process, SMC will allow positioning errors of 5 per cent with motions of the order of micrometres. Ando *et al.* [**21**] reported a chattering-free sliding-mode friction estimator and compensator for a mechanical instrument that assists a human operator to operate micro tasks, such as assembly or manufacturing. Wang *et al.* [**22**] demonstrated high accuracy in an *X–Y* positioning table with dry friction, using a combination of SMC and adaptive control. However, the SMC method has not been demonstrated to be effective for a braking–clutching mechanism used for position or trajectory control.

3.1 Proportional–derivative control development

The error $e(t)$ of the system is defined as the difference between the desired position $\theta_{\mathrm{d}}(t)$ and the measured position $\theta(t)$, shown in Fig. 2, according to

$$e(t) = \theta_{\mathrm{d}}(t) - \theta(t) \tag{3}$$

This error is used to compute the PD control law for the input $u(t)$ as

$$u(t) = K_{\mathrm{p}} e(t) + K_{\mathrm{d}} \frac{\mathrm{d}}{\mathrm{d}t} e(t) \tag{4}$$

where K_{p} and K_{d} are the controller gains. The derivative of the error with respect to time is approximated using the Kalman filter [**29**] according to

$$\frac{\mathrm{d}}{\mathrm{d}t} e(t) = \dot{e}_k = (1 - K_{\mathrm{Kal}})\dot{e}_{k-1} + K_{\mathrm{Kal}} \frac{e_k - e_{k-1}}{T} \tag{5}$$

where K_{Kal} is between 0.2 and 1 and denotes the Kalman constant, and T represents the chosen sampling time. The controller gains K_{p} and K_{d} are optimized through trial and error and their values are set to $K_{\mathrm{p}} = 5000$ and $K_{\mathrm{d}} = 50$.

3.2 Computed-torque control development

The CTC method assumes that the planned trajectory $\theta_{\mathrm{d}}(t)$ is sufficiently smooth that it has at least two derivatives. It is an approach that makes direct use of the complete dynamic model of a system to cancel not only the effects of gravity but also the Coriolis force, the centrifugal force, friction, and the manipulator inertia tensor. From equation (1), the system acceleration can be written as

$$\ddot{\theta} = J^{-1}[MgR_{\mathrm{p}} - T_{\mathrm{f}}(\dot{\theta}) - C_{\mathrm{d}}\dot{\theta}] \tag{6}$$

Defining the control input function τ as

$$\tau = \ddot{e} = \ddot{\theta}_{\mathrm{d}} - J^{-1}[MgR_{\mathrm{p}} - T_{\mathrm{f}}(\dot{\theta}) - C_{\mathrm{d}}\dot{\theta}] \tag{7}$$

the frictional torque T_{f} is obtained as

$$T_{\mathrm{f}}(\dot{\theta}) = MgR_{\mathrm{p}} - J(\ddot{\theta}_{\mathrm{d}} - \tau) - C_{\mathrm{d}}\dot{\theta} \tag{8}$$

Equation (8) represents the CTC law. As a result, the control law for the input $u(t)$ is obtained as

$$u(t) = \frac{A_{\mathrm{lever}} R_{\mathrm{a}} r_{\mathrm{c}} [MgR_{\mathrm{p}} - J(\ddot{\theta}_{\mathrm{d}} - \tau) - C_{\mathrm{d}}\dot{\theta}]}{\mu(\dot{\theta}) r_{\mathrm{i}} K_{\mathrm{t}} A} \tag{9}$$

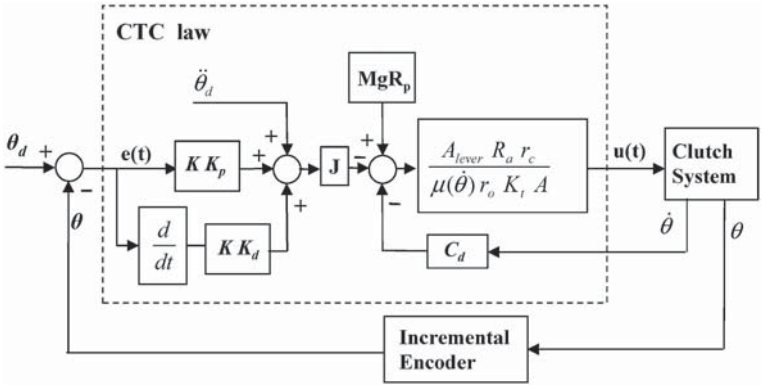

Fig. 3 System control diagram with CTC

The control input function τ is chosen as

$$\tau = -K\left[K_{\mathrm{p}}e(t) + K_{\mathrm{d}}\frac{\mathrm{d}}{\mathrm{d}t}e(t)\right] \tag{10}$$

where the error derivative was estimated using the Kalman filter given in equation (5). Substituting equation (10) into equation (9), the CTC law becomes

$$u(t) = \frac{A_{\mathrm{lever}}R_{\mathrm{a}}r_{\mathrm{c}}[MgR_{\mathrm{p}} - J(\ddot{\theta}_{\mathrm{d}} + KK_{\mathrm{p}}e + KK_{\mathrm{d}}\dot{e}) - C_{\mathrm{d}}\dot{\theta}]}{\mu(\dot{\theta})r_{\mathrm{i}}K_{\mathrm{t}}A} \tag{11}$$

The controller gains K, K_{p}, and K_{d} are optimized through trial and error and their values are set to $K = 90$, $K_{\mathrm{p}} = 100$, and $K_{\mathrm{d}} = 0.7$. The block diagram of the proposed clutch system with a CTC law is illustrated in Fig. 3.

3.3 Sliding-mode control development

A more robust method used for diminishing stick–slip within a mechanism with dry friction is SMC. To apply SMC, it is not necessary to know the exact system parameters, instead only bounds on these parameters can be used. Supposing that the planned trajectory $\theta_{\mathrm{d}}(t)$ shows no discontinuities, a state vector is defined as $\chi = [e, w]^{\mathrm{T}}$, where $e = \theta_{\mathrm{d}} - \theta$ and $w = \dot{e}$. From equation (1), the closed-loop equation of motion of the clutch system in terms of e and w can be given as

$$\begin{aligned} \dot{e} &= w \\ \dot{w} &= \ddot{e} = \ddot{\theta}_{\mathrm{d}} - J^{-1}\left[MgR_{\mathrm{p}} - \mu(\dot{\theta})\frac{r_{\mathrm{i}}K_{\mathrm{t}}A}{A_{\mathrm{lever}}R_{\mathrm{a}}r_{\mathrm{c}}}v_{\mathrm{a}}(t) - C_{\mathrm{d}}\dot{\theta}\right] \\ u &= f(e, w) \end{aligned} \tag{12}$$

The objective is to find an SMC law $u = f(e, w)$ such that the solution of the closed-loop system satisfies $\chi(t) \to 0$ as $t \to \infty$. SMC considers the linear constraint

$$\sigma(\chi) = fe + w = 0 \tag{13}$$

which is called the *sliding surface*. The parameter f is a positive defined constant called the sliding-mode gain. The sliding-mode gain f determines the speed of convergence of the tracking error e to zero during the sliding-mode regime defined by $\sigma(\chi)$. Thus, when the system is in the sliding mode, the tracking error is independent of the system parameters. The solution depends only on the sliding-mode gain. This property of SMC makes it ideal for controlling plants that operate in presence of unmodelled dynamics, parametric uncertainties, external disturbances, and noise. The sliding surface design is shown in Fig. 4.

To develop a control law $u = f(\chi)$ which will ensure that the system operates in the sliding mode, consider the Lyapunov-type function [**28**]

$$V_{\mathrm{L}}(\chi) = \frac{\sigma^{\mathrm{T}}(\chi)\sigma(\chi)}{2} \tag{14}$$

This is a Lyapunov-type function in the sense that $V_{\mathrm{L}}(\chi)$ is continuously differentiable, $V_{\mathrm{L}}(\chi) \geqslant 0$, and $V_{\mathrm{L}}(\chi) = 0 \to \textit{if and only if} \to \sigma(\chi) = 0$. Robust stability and good performance are guaranteed if all

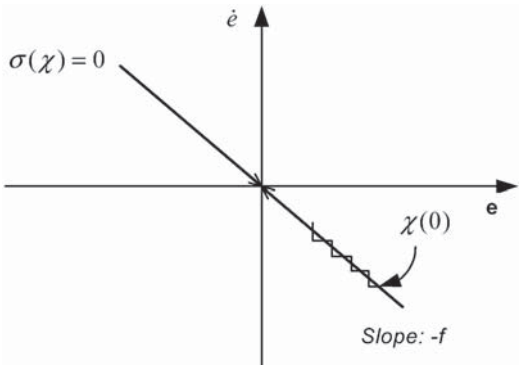

Fig. 4 Sliding surface design

trajectories are guaranteed to converge to the sliding surface given in equation (13). To show that the solution of the closed-loop system approaches the switching surface, it is sufficient to show that there is a solution for equation (12) as well as that $\dot{V}_L(\chi(t)) \leqslant 0$, and $\dot{V}_L(\chi(t)) \equiv 0$ implies that $\sigma(\chi(t)) \equiv 0$, where $\dot{V}_L(\chi) = \sigma^T(\chi)\dot{\sigma}(\chi)$. This condition guarantees that the solution approaches the switching surface in the limit as $t \to \infty$. To ensure that the solution of the closed-loop system hits the switching surface in a finite time, a somewhat stronger condition needs to be defined. Thus, if there exists a $\gamma > 0$ such that $\sigma^T(\chi)\dot{\sigma}(\chi) \leqslant -\gamma||\sigma(\chi)||$ together with a solution of equation (12), then $\chi(t)$ will hit the switching surface at time t_{switch}, where

$$t_{switch} \leqslant \frac{||\sigma(\chi(0))||}{\gamma} \tag{15}$$

The proof has been demonstrated in reference [**28**]. Thus, if $V_L(\chi(t))$ decreases at a rate proportional to $||\sigma(\chi(t))||$, the solution of equation (12) will strike the switching surface within a time that is bounded from above by t_{switch}. Once $\chi(t)$ reaches the switching surface, the dynamics that brought it there will also keep it there.

Differentiating the sliding surface given in equation (13) the equation

$$\dot{\sigma}(\chi) = f\dot{e} + \dot{w} = f\dot{e} + \ddot{\theta}_d - \ddot{\theta} \tag{16}$$

is obtained. Equation (16) can be written more explicitly as

$$\dot{\sigma}(\chi) = f\dot{e} + \ddot{\theta}_d - J^{-1} \times \left[MgR_p - \mu(\dot{\theta}) \frac{r_i K_t A}{A_{lever} R_a r_c} v_a(t) - C_d \dot{\theta} \right] \tag{17}$$

or

$$\dot{\sigma}(\chi) = f\dot{e} + \ddot{\theta}_d - J^{-1}[MgR_p - \mu(\dot{\theta}) K_{COF} v_a(t) - C_d \dot{\theta}] \tag{18}$$

where $K_{COF} = r_i K_t A/(A_{lever} R_a r_c)$ represents a constant of the frictional torque.

Equation (18) can be rewritten as

$$\dot{\sigma}(\chi) = \left[v_a(t) + \frac{C_d \dot{\theta}}{\mu(\dot{\theta}) K_{COF}} + \frac{J\ddot{\theta}_d}{\mu(\dot{\theta}) K_{COF}} - \frac{MgR_p}{\mu(\dot{\theta}) K_{COF}} + \frac{Jf\dot{e}}{\mu(\dot{\theta}) K_{COF}} \right] \frac{\mu(\dot{\theta}) K_{COF}}{J} \tag{19}$$

To show that $\dot{V}_L(\chi(t)) \leqslant 0$, and that $\dot{V}_L(\chi(t)) \equiv 0$ implies that $\sigma(\chi(t)) \equiv 0$, the equation

$$\sigma(\chi)\dot{\sigma}(\chi) = \sigma(\chi) \frac{\mu(\dot{\theta}) K_{COF}}{J} \times \left[v_a(t) + \frac{C_d \dot{\theta}}{\mu(\dot{\theta}) K_{COF}} + \frac{J\ddot{\theta}_d}{\mu(\dot{\theta}) K_{COF}} - \frac{MgR_p}{\mu(\dot{\theta}) K_{COF}} + \frac{Jf\dot{e}}{\mu(\dot{\theta}) K_{COF}} \right] \tag{20}$$

$$= |\sigma(\chi)| \frac{\mu(\dot{\theta}) K_{COF}}{J} v_a(t) + |\sigma(\chi)| \times \left(\frac{C_d \dot{\theta}}{J} - \frac{MgR_p}{J} + \ddot{\theta}_d + f\dot{e} \right) \tag{21}$$

is calculated and using $\theta = \theta_d - e$ gives

$$\sigma(\chi)\dot{\sigma}(\chi) = |\sigma(\chi)| \frac{\mu(\dot{\theta}) K_{COF}}{J} v_a(t) + |\sigma(\chi)| \left[\frac{C_d \dot{\theta}_d}{J} - \frac{MgR_p}{J} + \ddot{\theta}_d + \frac{(Jf - C_d)\dot{e}}{J} \right] \tag{22}$$

The bounds on the system given in equation (18), including the rate of change in the reference trajectory, are

$$0 < J_0 < J < J_1 \tag{23a}$$

$$(MgR_p)_1 < (MgR_p) < (MgR_p)_2 \tag{23b}$$

$$C_d < C_{d1} \tag{23c}$$

$$\mu_{min} \leqslant \mu_d \leqslant \mu_{d1} \tag{23d}$$

$$\mu_{min} \leqslant \mu_s \leqslant \mu_{s1} \tag{23e}$$

$$|\mu(\dot{\theta})| < \mu_{s1} + \mu_{d1} \tag{23f}$$

$$|\dot{\theta}_d| < v_d, |\ddot{\theta}_d| < a_d \tag{23g}$$

$$K_{COF1} < K_{COF} < K_{COF2} \tag{23h}$$

where J_0, J_1, $(MgR_p)_1$, $(MgR_p)_2$, C_{d1}, μ_{s1}, μ_{d1}, v_d, a_d, K_{COF1}, and K_{COF2} are positive defined constants.

Thus, equation (22) can be rewritten as

$$\sigma(\chi)\dot{\sigma}(\chi) \leqslant |\sigma(\chi)| \frac{(\mu_{s1} + \mu_{d1}) K_{COF2}}{J_0} v_a(t) + |\sigma(\chi)| \left[\frac{C_{d1} v_d}{J_0} - \frac{(MgR_p)_1}{J_0} + a_d + \frac{(J_1 f - C_{d1})\dot{e}}{J_0} \right] \tag{24}$$

Selecting the SMC law as

$$v_a(t) = u(t) = -\{K_p \operatorname{sgn}[\sigma(\chi)] + K_d \operatorname{sgn}[\sigma(\chi)\dot{e}]\,\dot{e}\} \tag{25}$$

the positive defined controller gains K_p and K_d are obtained as

$$K_p > \frac{J_0 a_d + C_{d1} v_d - (MgR_p)}{(\mu_{s1} + \mu_{d1})K_{COF2}} \tag{26}$$

$$K_d > \frac{J_1 f - C_{d1}}{(\mu_{s1} + \mu_{d1})K_{COF2}} \tag{27}$$

The constant γ is obtained from $\sigma(\chi)\dot{\sigma}(\chi) \leqslant -\gamma\|\sigma(\chi)\|$ as

$$\gamma = \frac{K_p(\mu_{s1} + \mu_{d1})K_{COF2} - J_0 a_d + C_{d1} v_d - (MgR_p)_1}{J_0} \tag{28}$$

The resulting controller is given as

$$\sigma(\chi) = fe + \dot{e}$$

$$K_p > \frac{J_0 a_d + C_{d1} v_d - (MgR_p)_1}{(\mu_{s1} + \mu_{d1})K_{COF2}}$$

$$K_d > \frac{J_1 f - C_{d1}}{(\mu_{s1} + \mu_{d1})K_{COF2}}$$

$$v_a(t) = u(t) = -\{K_p \operatorname{sgn}[\sigma(\chi)] + K_d \operatorname{sgn}[\sigma(\chi)\dot{e}]\,\dot{e}\} \tag{29}$$

This controller can cause excessive high-frequency oscillations due to the discontinuous characteristics of the control input. To reduce this oscillation, the function signum in equation (29) is replaced by the saturation function

$$\operatorname{sat}\left(\frac{\sigma}{\varepsilon}\right) = \begin{cases} \operatorname{sgn}\left(\dfrac{\sigma}{\varepsilon}\right), & \text{if } |\sigma| \geqslant \varepsilon, \\ \dfrac{\sigma}{\varepsilon}, & \text{if } |\sigma| < \varepsilon \end{cases} \tag{30}$$

where ε is a positive term that defines the thickness of the boundary layer as shown in Fig. 5.

Thus, equation (29) can be written as

$$\sigma(\chi) = fe + \dot{e}$$

$$K_p > \frac{J_0 a_d + C_{d1} v_d - (MgR_p)_1}{(\mu_{s1} + \mu_{d1})K_{COF2}}$$

$$K_d > \frac{J_1 f - C_{d1}}{(\mu_{s1} + \mu_{d1})K_{COF2}}$$

$$v_a(t) = u(t) = -\left\{K_p \operatorname{sat}\left[\frac{\sigma(\chi)}{\varepsilon}\right] + K_d \operatorname{sat}\left[\frac{\sigma(\chi)\dot{e}}{\varepsilon}\right]\dot{e}\right\} \tag{31}$$

The SMC block diagram illustration of the above equation (31) is shown in Fig. 6, and the controller gains chosen for all the three controllers are listed in Table 2.

4 RESULTS AND DISCUSSION

To investigate the performance of each controller, simulations and experiments were performed. Simulations were performed using the MATLAB and Simulink package. A sampling rate of 1 ms was chosen, and the solver used is based on the explicit

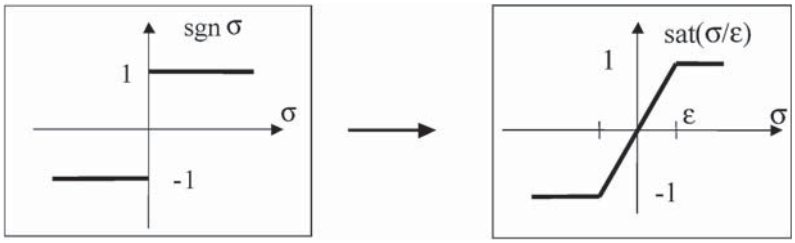

Fig. 5 Saturation function

Table 2 Controller design parameters

	Controller parameters				
Controller	K_p	K_d	K	f	ε
PD controller	5000	50	–	–	–
Computed-torque controller	100	0.7	90	–	–
Sliding-mode controller	3	400	1	70	0.1

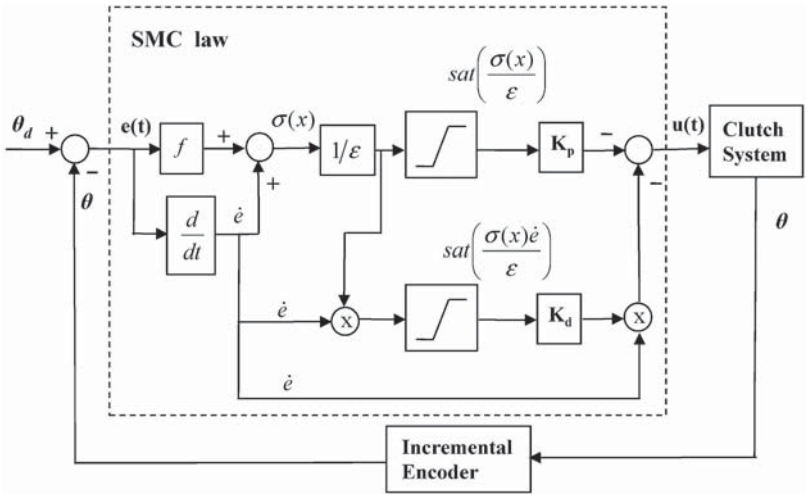

Fig. 6 SMC block diagram

Runge–Kutta formula (4) and (5), the Dormand–Prince pair. The experiments were performed using the computational workstation for real-time control illustrated in Fig. 7. The computational workstation is a Pentium 233 MHz personal computer (PC) running the QNX real-time operating system. The control output is sent via a 12-bit digital-to analogue converter. The control algorithms are implemented using a control development studio developed by Reedman [**30**]. A 126 W brushless (permanent magnet) d.c. motor capable of producing approximately 5 N m of torque is used. The position sensor employed is an incremental encoder which generates, via an electronic interface, 20 000 counts/rev, giving a resolution of 0.018°. The sample frequency is set to 1 kHz using a PC 14 AT Amplicon Liveline board.

The controllers developed in section 3 are investigated and evaluated in this section. A constant driving torque of 0.047 N m is used. The desired position has been chosen as a ramp with different

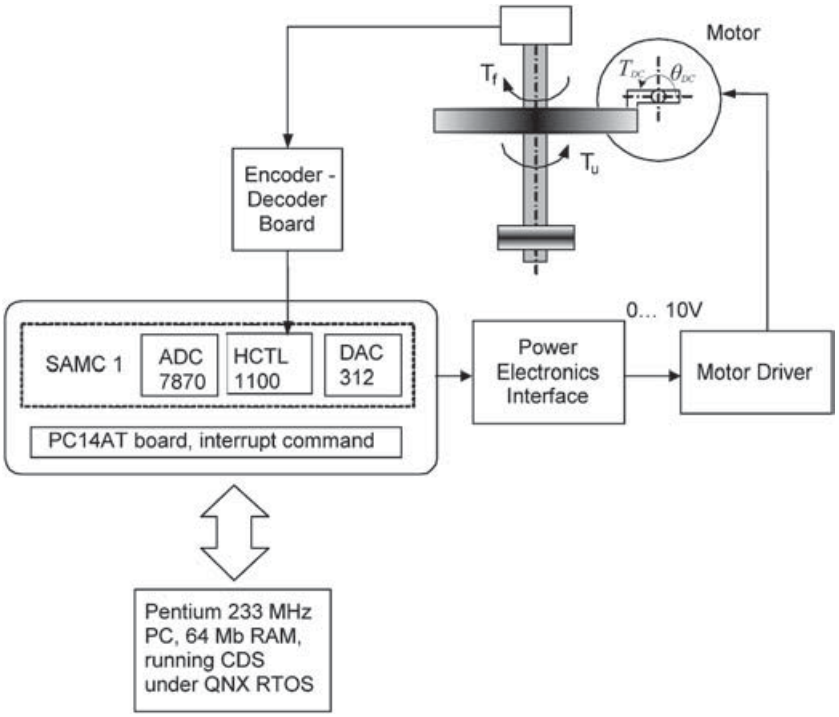

Fig. 7 Computational workstation overview (ADC, analogue-to-digital converter; DAC, digital-to-analogue converter; PC, personal computer; RAM, random-access memory; CDS, control development studio; RTOS, real-time operating system)

gradients (i.e. position rates). The aim of the investigation is to control the motion of the clutch shaft smoothly and accurately for a position rate of 2°/s.

4.1 Results with the PD controller

Figures 8(a) and (b) show the simulation and experimental results respectively with the PD controller developed in equation (4), where the desired path gradient (i.e. position rate) is set to 100, 20, and 2°/s respectively. From Fig. 8 it can be seen that for a position rate greater than 20°/s the position is smoothly controlled, without any discontinuities, and thus without stick–slip. A positional error of under 0.12° is demonstrated in both simulation and experimental results. As the position rate decreases below 20°/s, the PD controller can no longer contribute to cancelling the stick–slip phenomenon, which is highly noticeable. This is illustrated in both simulation (Fig. 8(a)) and experiment (Fig. 8(b)) for a position rate of 2°/s. Thus, for a position rate of 2°/s, even though the position error is minimal (0.04° from the simulation analysis and 0.08° from the experimental analysis), the clutch motion is discontinuous, which introduces undesired vibrations in the system.

4.2 Results with CTC

It was shown in the above section that a PD controller can successfully compensate for stick–slip for velocities greater than 20°/s. However, it is required to control the system's motion for velocities much lower than 20°/s; thus a better controller is required to reduce stick–slip for velocities between 2 and 20°/s. The CTC law derived in equation (11) was implemented in both simulations and experimental set-ups. Figures 9(a) and (b) show the simulation and experimental results respectively, where the desired path gradient is set to 20 and 2°/s. From the simulation results shown in Fig. 9(a) it can be seen that the CTC method is able to compensate successfully for stick–slip for a velocity of 2°/s, keeping the error at the limit of the encoder resolution. This observation is also true for any velocity above 2°/s, as demonstrated for a velocity of 20°/s in Fig. 9(a). However, from the experimental results shown in Fig. 9(b), it can be seen that a different performance of the clutch system is obtained. The scale difference on the x and y axes in Figs 9(a) and (b) has been chosen as shown for clarity.

From the experimental results shown in Fig. 9(b), it can be seen that the system exhibits stick–slip for a velocity of 2°/s. This is also true for any position rate less than 20°/s. Furthermore, it can be seen that the positional error is much higher than that obtained from the simulation analysis. This discrepancy between the simulation and experimental results arises because the simulations were performed assuming a perfect knowledge of the system parameters (friction-related parameters in particular), whilst the real friction is very difficult to model accurately. However, if the system friction can be accurately measured or exactly estimated, as shown in the simulation analysis, the CTC law is demonstrated to have the potential to achieve minimum

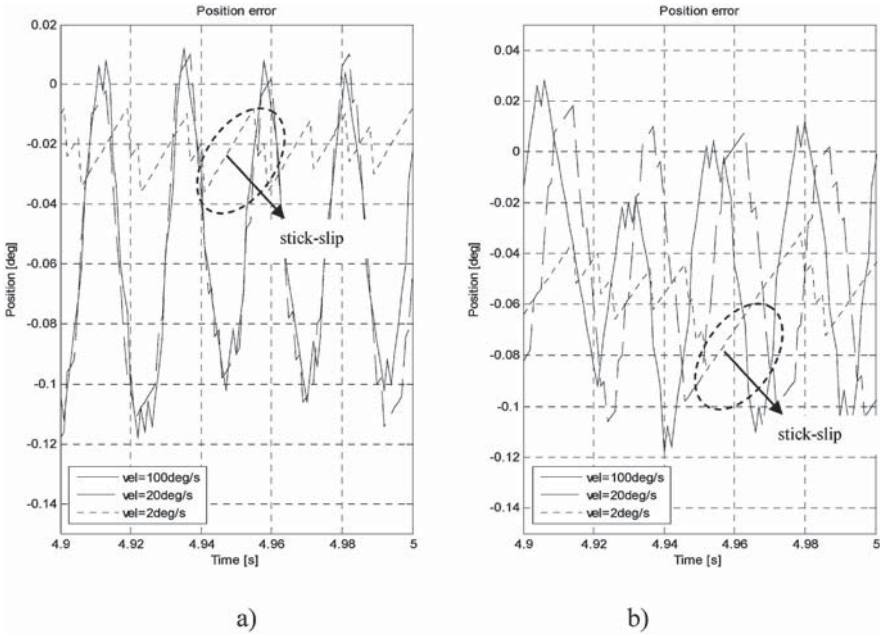

Fig. 8 Positional errors with the PD controller: (a) simulation results; (b) experimental results

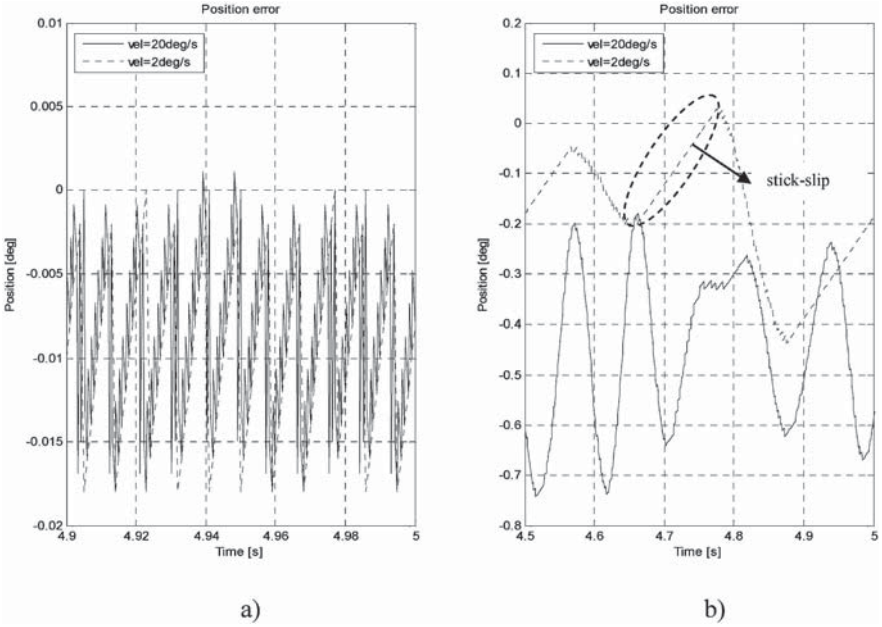

Fig. 9 Positional errors with the computed-torque controller: (a) simulation results; (b) experimental results

error while avoiding stick–slip for velocities as low as 2°/s.

4.3 Results with SMC

The SMC law derived in section 3.3 was implemented in both simulation and experimental set-ups with the aim of cancelling or reducing the stick–slip effect for a velocity of 2°/s. Figures 10(a) and (b) show the simulation and experimental results respectively, where the desired path gradient is set to 20, 6, and 2°/s. From the simulation results shown in Fig. 10(a) it can be seen that the SMC method is able to reduce successfully stick–slip for all velocities illustrated including a velocity of 2°/s. Moreover, the positional error is kept below 0.15°, which is satisfactory.

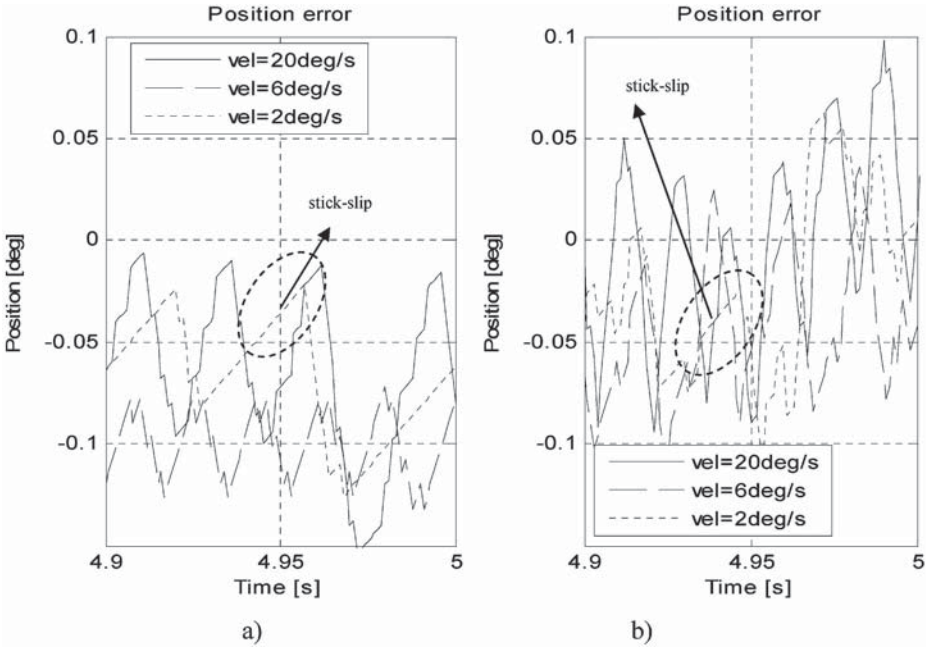

Fig. 10 Positional errors with the sliding-mode controller: (a) simulation results; (b) experimental results

The experimental results obtained using the SMC law are shown in Fig. 10(b). It can be seen that, even though stick–slip occurs for velocities of 2 and 6°/s, it is much reduced in comparison with the results for the PD controller. A comparison between the experimental results obtained with the PD controller and SMC is given in Table 3. The stick–slip reduction is presented in percentages and is calculated from

$$\text{SMC versus PD}_{\text{stick–slip}}\,(\text{per cent}) = 100\frac{\text{SMC}_{\text{stick–slip}}}{\text{PD}_{\text{stick–slip}}} \tag{32}$$

where $\text{SMC}_{\text{stick–slip}}$ and $\text{PD}_{\text{stick–slip}}$ represent the number of stick–slip cycles during 1 s. For example, if, with a PD controller, 100 stick–slip limit cycles occur in $t = 1$ s and if, with a sliding-mode controller, 11 stick–slip limit cycles occur in the same time, a reduction of 89 per cent is obtained. The stick–slip percentage was averaged from ten measurements and the results are given in Table 3.

5 CONCLUSIONS

In applications such as robotic assistance in surgery, which involve close interaction between a robotic or mechatronic device and humans, safety is a major design constraint. Such a safety requirement can be addressed by allowing the user to move the end effector while the motion of the end effector is constrained to a pre-planned trajectory or region, using computer-controlled clutch-type joints. However, at low velocities a periodic process of sticking and sliding (i.e. stick–slip) is inherent in friction-type mechanisms. Three controllers capable of diminishing the stick–slip effect were developed and investigated. With a PD controller for velocities greater than 20°/s, it can be seen that stick–slip was successfully compensated for. The CTC method also proved to be very efficient as long as exact system parameters are assumed. This is shown in the simulations, where it is illustrated that, besides fully avoiding the stick–slip effect, even for a position rate of 2°/s, the controller is capable of tracking the position at the limit of the encoder resolution. However, exact values of the system parameters are rarely available in practice; thus the experimental analysis suffers from the sensitivity to errors in the estimates of these parameters.

Table 3 Stick–slip comparison for experimental results with constant torque

Velocity	Reduction in stick–slip for SMC compared with PD control (%)
$\dot{\theta}_d = 10°/s$	88.6
$\dot{\theta}_d = 6°/s$	88.9
$\dot{\theta}_d = 2°/s$	83.8

A more robust approach is the SMC method where it is not necessary to know the system parameters exactly; instead only ranges of these parameters are needed. Using SMC it was demonstrated that the stick–slip effect was significantly reduced at low velocities. It was shown that for a velocity of 2°/s, the stick–slip reduction is very effective with a sliding-mode controller when compared with the results achieved with the PD controller. A reduction in stick–slip by as much as 89 per cent is demonstrated for a velocity of 6°/s, and a reduction of 84 per cent for a velocity of 2°/s. The superior performance of the SMC arises because, when the system is in the sliding mode, the tracking error is independent of the system parameters, while the PD controller is dependent on the system dynamics.

REFERENCES

1 **Armstrong-Hélouvry, B.** *Control of machines with friction*, 1991 (Kluwer, Norwell, Massachusetts).
2 **Leonard, N. E.** and **Krishnaprasad, P. S.** Adaptive friction compensation for bi-directional low-velocity position tracking. In Proceeding of the 31st IEEE Conference on *Decision and control*, Tucson, Arizona, USA, 1992, pp. 267–273 (IEEE, New York).
3 **Canudas de Wit, C., Noel, P., Aubin, A.,** and **Brogliato, B.** Adaptive friction compensation in robot manipulators: low velocities. *Int. J. Robotics Res.*, 1991, **10**, 189–199.
4 **Morel, G.** and **Dubowsky, S.** The precise control of manipulators with joint friction: a base force/torque sensor method. In Proceedings of the IEEE Conference on *Robotics and automation*, 1996, pp. 360–365 (IEEE, New York).
5 **Gitis, N. V.** Study of anti-stick–slip properties of machine tool guideway materials. *Soviet J. Friction Wear*, 1996, **7**, 72–76.
6 **Tung, E. D., Urushisaki, Y.,** and **Tomizuka, M.** Low velocity friction compensation for machine tool feed drives. In Proceedings of the Americal Control Conference, San Francisco, California, USA, 1993, pp. 1932–1936 (IEEE, New York).
7 **Younkin, G. W.** Modelling machine tool feed servo drives using simulation techniques to predict performance. *IEEE Trans. Industry Applic.*, 1991, **27**, 268–274.
8 **Book, W., Charles, R., Davis, R.,** and **Gomes, M.** The concept and implementation of a passive trajectory enhancing robot. In Proceedings of the ASME Dynamic Systems and Control Division, Vol. 58,

1996, pp. 633–638. (American Society of Mechanical Engineers, New York)
9 **Love, L. J.** and **Book, W.** Design and control of a multi-degree-of-freedom haptic interface. In Proceedings of the 1994 International Mechanical Engineering Congress and Exposition, Chicago, Illinois, USA, 6–11 November 1994, Vol. 2, pp. 851–856.
10 **Swanson, D. K.** and **Book, W.** Torque feedback control of dry friction clutches for a dissipative passive haptic interface. In Proceedings of the Ninth IEEE Conference on *Control applications*, Anchorage, Arkansas, USA, 2000, pp. 736–741 (IEEE, New York).
11 **Swanson, D. K.** and **Book, W.** Path-following control for dissipative passive haptic displays. In Proceedings of the 11th International Symposium on *Haptic interfaces for virtual environment and teleoperated systems*, Los Angeles, California, USA, 2003, pp. 101–108.
12 **Swanson, D. K.** and **Book, W.** Obstacle avoidance methods for a passive haptic display. In Proceeedings of the IEEE–ASME International Conference on *Advanced intelligent mechatronics*, Como, Italy, 2001, pp. 1187–1192 (IEEE, American Society of Mechanized Engineers, New York).
13 **Munir, S., Tognetti, L.,** and **Book, W.** Experimental evaluation of a new braking system for use in passive haptic displays. In Proceedings of the American Control Conference, San Diego, California, USA, 1999, pp. 4456–4460 (IEEE, New York).
14 **Armstrong-Helouvry, B., Dupont, P.,** and **Canudas de Wit, C.** A survey of models, analysis tools and compensation methods for the control of machines with friction. *Automatica*, 1994, **30**, 1083–1138.
15 **Dupont, P. E.** Avoiding stick–slip through PD control. *IEEE Trans. Autom. Control*, 1994, **39**, 1094–1097.
16 **Luh, J. Y. S., Fischer, W. D.,** and **Paul, R. P. C.** Joint torque control by a direct feedback for industrial robots. *IEEE Trans. Autom. Control*, 1983, **28**, 153–161.
17 **Pfeffer, L., Khatib O.,** and **Hake J.** Joint torque sensory feedback in the control of a PUMA manipulator. *IEEE Trans. Robotics Autom.*, 1989, **5**, 418–425.
18 **Hashimoto, M.** Robot motion control based on joint torque sensing. In Proceedings of the International Conference on *Robotics and automation*, 1989, pp. 256–261 (IEEE International, Scottsdale, USA).
19 **Wu, C. H.** and **Paul, R. P.** Manipulator compliance based on joint torque control. In Proceedings of the 19th Conference on *Decision and control*, Albuquerque, New Mexico, USA, 1980, pp. 89–94 (IEEE, New York).
20 **Lee, S.-B., Misawa, E. A.,** and **Lucca, D. A.** Sliding mode compensation of dry friction. In Proceedings of the Fifth IEEE Conference on *Control applications*, 1996, pp. 809–813 (IEEE, New York).
21 **Ando, N., Korondi, P., Hashimoto, H.,** and **Szemes, T.** Friction compensation for 6-DOF Cartesian coordinate haptic interface. In Proceedings of the IEEE International Conference on *Intelligent robots and systems*, 2002, Vol. 3, pp. 2893–2898 (IEEE, New York).
22 **Wang, Z., Wang, X.,** and **Xu, W.** Robust adaptive friction compensation for *X–Y* positioning table. *Dongnan Daxue Xuebao (Ziran Kexue Ban)/J. Southeast Univ.* (*Natural Sci. Edn*), 2002, **32**(1), 69–72.
23 **Hirel, P.** Adaptive optics, dither optimisation method in an adaptive optic model. *Proc. SPIE*, 1990, **1271**, 22–32.
24 **Chau, W. K.** A critical analysis of dithering algorithms for image processing. In Proceedings of the IEEE Region 10 Conference on *Computers and communication systems*, Hong Kong, PR China, 1990, pp. 309–313.
25 **Zames, G.** and **Shneydor, N. A.** Dither in nonlinear systems. *IEEE Trans. Autom. Control*, 1976, **21**, 660–667.
26 **Hojjat, Y.** and **Higuchi, T.** Application of electromagnetic impulsive force to precise positioning. *Int. J. Japan Soc. Precision Engng*, 1991, **25**, 39–44.
27 **Suzuki, A.** and **Tomizuka, M.** Design and implementation of digital servo controller for high speed machine tools. In Proceedings of the American Control Conference, Boston, Massachusetts, USA, 1991, pp. 1246–1251.
28 **Schilling, R. J.** *Fundamental of robotics: analysis and control*, 1990 (Prentice Hall, Englewood Cliffs, New Jersey).
29 **Ong, F. R.** *Analysis of bone drilling characteristics for the enhancement of safety and the evaluation of bone strength*. PhD Thesis, Loughborough University, 1998.
30 **Reedman, A. V. C.** *The design and control of a manipulator for safety critical deployment applications*. PhD Thesis, Loughborough University, 2002.

APPENDIX

Notation

A	area of the contact between the brake pad and the brake disc
A_{lever}	area of a rectangular shape of the mechanical lever
C_{d}	viscous damping coefficient in the system
$e(t)$	position error
f	sliding-mode control gain
F_{N}	normal force on the braking disc
g	gravitational acceleration
J	total moment of inertia
K	controller constant
K_{d}	derivative gain
K_{COF}	constant of the coefficient of friction
K_{Kal}	design parameter for Kalman filtering
K_{p}	proportional gain
K_{t}	motor torque constant
M	mass released on pulley
r_{c}	distance between centre of the motor shaft and contact point on the disc.

r_i	inner radius of the brake disc
r_o	radius of the brake disc
R_a	armature resistance
R_p	pulley radius
t	time
T	sampling time
T_{DC}	motor torque
T_f	frictional torque
T_u	driving torque
u	input for the control law
v_a	armature voltage
δ	Stribeck coefficient
ε	thickness of the boundary layer used for saturation
θ	angular shaft position
$\dot{\theta}$	angular shaft velocity
$\ddot{\theta}$	angular shaft acceleration
θ_d	desired position
$\dot{\theta}_S$	Stribeck velocity
θ_{DC}	motor shaft position
$\dot{\theta}_{DC}$	motor shaft velocity
$\ddot{\theta}_{DC}$	motor shaft acceleration
μ	coefficient of friction
μ_d	dynamic friction coefficient
μ_s	static friction coefficient
$\sigma(\chi)$	sliding surface for the sliding-mode controller
τ	control input function